to systematic errors. Samples were prepared in precision NMR tubes, degassed three times, and sealed.

2-Butanone-*1,1,1,3,3-d*$_5$. 2-Butanone (10 mL; Aldrich Chemical Co.), Na_2CO_3 (0.1 g), and D_2O (20 mL; Aldrich Chemical Co.) were placed into a 100-mL flask equipped with a stirring bar, reflux condenser, and drying tube. The mixture was allowed to reflux for 24 h at which time the 2-butanone was separated from the D_2O by salting out and distilling. The exchange procedure was performed five times. NMR analysis revealed 99.7% deuterium incorporation.

Methylamine-*N,N-d*$_2$ Deuteriochloride. Methylamine hydrochloride (50.0 g; Pfalz and Bauer, Inc.), and D_2O (50 mL; Aldrich Chemical Co.) were placed in a flask equipped with a stirring bar, reflux condenser, and drying tube. The mixture was refluxed for 24 h at which time the D_2O was removed at reduced pressure. The exchange procedure was performed six times. NMR analysis revealed 99.5% deuterium incorporation.

***N*-Methyl-2-aminobutane-*1,1,1,2,3,3-d*$_6$.** 2-Butanone-*1,1,1,3,3-d*$_5$ (2.69 mL), methylamine-*N,N-d*$_2$ deuteriochloride (10.13 g), and sodium cyanoborodeuteride (1.88 g; Aldrich Chemical Co.) in 75 mL of methanol-d_1 were stirred for 72 h at 298 K. The solution was cooled while concentrated HCl was added until the pH was less than 2. The methanol was removed by distillation. The residue was taken up in 10 mL of water and extracted with 20-mL portions of ether. The aqueous solution was cooled and brought to a pH greater than 10 with solid KOH, saturated with NaCl, and extracted with five 15-mL portions of ether. The combined extracts were dried ($MgSO_4$), and the ether was removed on the spinning band column. The residue was distilled with a short path column (yield: 1.5 g; 57.5%). Characterization was done by ^{1}H NMR.

***N*-Methyl-*d*$_3$-2-aminobutane-*4,4,4-d*$_3$** was prepared by the same procedure used for *N*-methyl-2-aminobutane-*1,1,1,2,3,3-d*$_6$, except that 2-butanone-*4,4,4-d*$_3$ (2.69 mL; MSD Isotopes), methyl-d_3-amine hydrochloride (10.125 g; Aldrich Chemical Co.), sodium cyanoborohydride (1.88 g; Aldrich Chemical Co.), and methanol were used.

***N*-Methyl-2-aminobutane-*1,1,1,3,3-d*$_5$** was prepared by the same procedure used for *N*-methyl-2-aminobutane-*1,1,1,2,3,3-d*$_6$, except that sodium cyanoborohydride (1.88 g; Aldrich Chemical Co.) was used.

***N*-Ethyl-*2,2,2-d*$_3$-*N*-methyl-*d*$_3$-2-aminobutane-*1,1,1,2,3,3-d*$_6$ (1).** Benzene (1 mL) and 50% NaOH (4 mL) were added to a 10-mL round-bottom flask equipped with a magnetic stirring bar and stopper. *N*-Methyl-d_3-2-aminobutane-*1,1,1,2,3,3-d*$_6$ (2.0 mL, 0.006 mol) and iodoethane-*2,2,2-d*$_3$ (1 g, 0.006 mol; MSD Isotopes) were added to the benzene layer. The reaction mixture was stirred for 72 h. The reaction mixture was then poured into a test tube and centrifuged, and the clear layer was removed by pipette. The product was purified on a 5% XE-60/25% SF-96 Chromosorb W GLPC column (20 ft by 3/8 in.). Characterization was done by ^{1}H NMR, mass spectrometry, and comparison of the GC retention time with that of the non-deuteriated compound. ^{1}H NMR: See Figures 1–4 and Table I.

***N*-Ethyl-*1,1-d*$_2$-*N*-methyl-2-aminobutane-*1,1,1,3,3-d*$_5$ (2)** was prepared by the same procedure used for **1** except that *N*-methyl-2-aminobutane-*1,1,1,3,3-d*$_5$ (2.0 mL, 0.006 mol) and iodoethane-*1,1-d*$_2$ (1 g, 0.006 mol; MSD Isotopes) were used. Characterization was done by ^{1}H NMR, mass spectrometry, and comparison of the GC retention time with that of the all hydrogen compound. ^{1}H NMR: See Figures 5 and 6 and Table III.

***N*-Ethyl-*d*$_5$-*N*-methyl-*d*$_3$-2-aminobutane-*4,4,4-d*$_3$ (3)** was prepared by the same procedure used for **1** except that *N*-methyl-d_3-2-aminobutane-*4,4,4-d*$_3$ (2.0 mL, 0.006 mol) and iodoethane-d_5 (1 g, 0.006 mol; MSD Isotopes) were used. Characterization was done by ^{1}H NMR, mass spectrometry, and comparison of the GC retention time with that of the all-hydrogen compound. ^{1}H NMR: See Figures 7–10 and Tables IV and V.

Acknowledgment. C.H.B. is grateful to the National Science Foundation for support (Grant CHE80-24931 and CHE83-06876). We appreciate the assistance of the University of Vermont Academic Computing Center staff in providing outstanding computational support. We also appreciate assistance with the molecular mechanics calculations from Christine Dimeglio.

Supplementary Material Available: Tables of bond angles and dihedral angles for the R_CR_N/S_CS_N and R_CS_N/S_CR_N families of conformations calculated by using Allinger's 1980 MM2 molecular mechanics force field (4 pages). Ordering information is given on any current masthead page.

Intermolecular Electronic Interactions in the Primary Charge Separation in Bacterial Photosynthesis

M. Plato,[†] K. Möbius,[†] M. E. Michel-Beyerle,[‡] M. Bixon,[§] and Joshua Jortner*,[§]

Contribution from the Institut für Molekülphysik, Freie Universität Berlin, Arnimallee 14, 1000 Berlin 33, FRG, and Institut für Physikalische und Theoretische Chemie, Technische Universität München, Lichtenbergstrasse 4, Garching, FRG, and the School of Chemistry, Sackler Faculty of Exact Sciences, Tel Aviv University, 69 978 Tel Aviv, Israel.
Received November 24, 1987

Abstract: In this paper we utilize the intermolecular overlap approximation to calculate the relative magnitudes of the electronic transfer integrals between the excited singlet state (^{1}P*) of the bacteriochlorophyll dimer (P) and the accessory bacteriochlorophyll (B) and between B$^-$ and bacteriopheopytin (H), along the L and M subunits of the reaction center (RC) of *Rps. viridis*. The ratio of the electron-transfer integrals for $B_L^-H_L-B_LH_L^-$ and for $B_M^-H_M-B_MH_M^-$ was calculated to be 2.1 ± 0.5, which together with the value of 2.8 ± 0.7 for the ratio of the transfer integrals for $^1P^*B_L-P^+B_L^-$ and for $^1P^*B_M-P^+B_M^-$ results in the electronic contribution of 33 ± 16 to the ratio k_L/k_m of the rate constants k_L and k_M for the primary charge separation across the L and M branches of the RC, respectively. The asymmetry of the electronic coupling terms, which originates from the combination of the asymmetry in the charge distribution of ^{1}P* and of structural asymmetry of the P–B and B–H arrangements across the L and M subunits, provides a major contribution to the unidirectionality of the charge separation in bacterial photosynthesis. A significant contribution to the transfer integrals between adjacent pigments originates from nearby methyl groups through hyperconjugation. The ratio 6 ± 2 of the transfer integrals for $^1P^*B_L-P^+B_L^-$ and for $B_L^-H_L-B_LH_L^-$ was utilized to estimate the energetic parameters required to ensure the dominance of the superexchange mediated unistep electron transfer $^1P^*BH \rightarrow P^+BH^-$ over the thermally activated $^1P^*B \rightarrow P^+B^-$ process.

I. Introduction

The conversion of solar energy into photochemical energy in reaction centers (RC) of photosynthetic bacteria proceeds via a sequence of well-organized, highly efficient, directional, and specific electron-transfer steps across the photosynthetic membrane.[1-3] The electron-transfer processes involve various pigments

[†] Institut für Molekülphysik, Freie Universität Berlin.
[‡] Institut für Physikalische und Theoretische Chemie, Technische Universität München.
[§] Tel Aviv University.

(1) Deisenhofer, J.; Epp, O.; Miki, K.; Huber, R.; Michel, H. *J. Mol. Biol.* **1984**, *180*, 385.
(2) Deisenhofer, J.; Epp, O.; Miki, K.; Huber, R.; Michel, H. *Nature (London)* **1985**, *318*, 618.

0002-7863/88/1510-7279$01.50/0

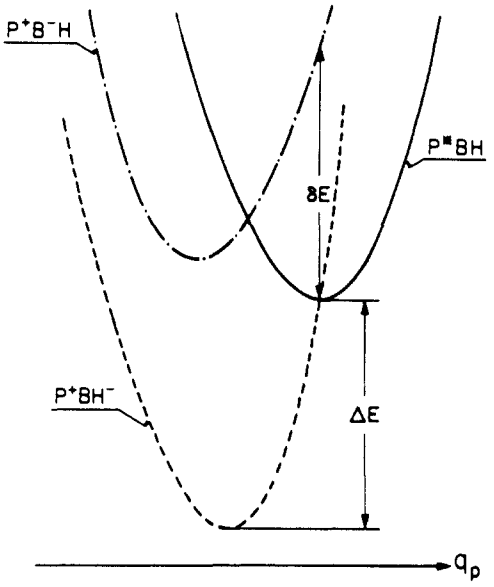

Figure 1. Nuclear potential energy surfaces for the superexchange electronic interaction mechanism in the RC.

arranged in their native protein matrix. Of central importance is the primary charge separation process with a rate $k = 3.7 \times 10^{11}$ s^{-1} at 295 K occurring from the excited singlet state (^{1}P*) of the bacteriochlorophyll dimer (P) to the bacteriopheophytin (H),[4,5] which constitutes the first identified electron acceptor. The ultrafast rate for the primary charge separation process over a center-to-center distance of 17 Å implies the involvement of the accessory bacteriochlorophyll (B), which is located between P and H, either as a genuine short lived ionic kinetic intermediate or by the modification of the ^{1}P*–H electronic coupling via superexchange interactions. Two classes of mechanisms were advanced for the primary charge separation process: (i) two-step sequential electron transfer, which involve the intermediate P$^+$B$^-$H[6] or PB$^+$H$^-$,[7] whose lifetime is shorter than the current experimental temporal resolution (~100 fs); and (ii) one-step direct electron transfer ^{1}P*BH → P$^+$BH$^-$, which is mediated by superexchange electronic interactions via the virtual states of P$^+$B$^-$H.[8,9] On the basis of an analysis of the magnetic data for the magnitude $J \simeq 10^{-3}$–10^{-4} cm^{-1} [10] and the temperature independence (in the range 300 K–80 K) of the exchange integral for the P$^+$H$^-$ radical pair in quinone depleted RCs, of *Rb. sphaeroides*,[11,12] in conjunction with the activationless nature of the primary charge separation process,[13-15] we have demonstrated[16a,b] that the sequential mechanisms (i) are inapplicable. Marcus has advanced[6c,d] a nonadiabatic/adiabatic mechanism for the primary process, while we have concluded[16b,c] that the unistep, superexchange mediated mechanism (ii) should be favored.

The electron-transfer rate constant is[17-19]

$$k = \frac{2\pi}{\hbar} V^2 F \qquad \text{(I.1)}$$

where F is the thermally averaged Franck–Condon nuclear overlap factor and V is the electronic interaction term. Provided that the frequencies of the nuclear modes ($\hbar\omega = 100$ cm^{-1}) of the protein medium are low compared to the thermal energy k_BT, the classical high-temperature limit of F is given by the Marcus relation[18,19]

$$F = (4\pi\lambda k_BT)^{-1/2} \exp(-E_a/k_BT) \qquad \text{(I.2)}$$

where λ is the medium reorganization energy and

$$E_a = (\Delta G - \lambda)^2/4\lambda k_BT \qquad \text{(I.3)}$$

is the activation energy, with ΔG being the free energy of the reaction. The electronic coupling V is attributed to superexchange. Figure 1 describes the superexchange interaction between the lowest vibronic level of ^{1}P*BH, with the quasi-isoenergetic vibronic manifold of the P$^+$BH$^-$ state being mediated by the off-resonance coupling of ^{1}P*BH with the vibronic manifold of the P$^+$B$^-$H state. When the energy differences between ^{1}P*BH states and the P$^+$B$^-$H mediating states effectively coupled to it exceed the average vibrational spacing ($\hbar\omega = 100$ cm^{-1}) of the protein medium, the electronic coupling assumes the form[8,9]

$$V = V_{PB}V_{BH}/\delta E \qquad \text{(I.4)}$$

$$V_{PB} = \langle\psi_P|\hat{H}|\psi_B\rangle \qquad V_{BH} = \langle\psi_B|\hat{H}|\psi_H\rangle \qquad \text{(I.5)}$$

where ψ_P, ψ_B, and ψ_H denote the electronic wave functions for ^{1}P*BH, P$^+$B$^-$H, and P$^+$BH$^-$, respectively. $\hat{H}$ is the Hamiltonian of the system. δE is the vertical energy difference between the potential surfaces for ^{1}P*BH and P$^+$B$^-$H at the intersection point of the potential surfaces of ^{1}P*BH and P$^+$BH$^-$ (Figure 1).

The evaluation of the intermolecular electron-transfer integrals, eq I.4 and I.5, is of considerable interest for two reasons. First, the unidirectionality of the primary charge separation process in the RC, which proceeds via the L branch,[4,5,7,9c] poses a real theoretical challenge. Recently[8] we have evaluated the electronic coupling terms V_{PB} across the L and M branch, demonstrating that small effects of structural asymmetry between P–B$_L$ and P–B$_M$ go a long way to result in a gross modification of the electronic coupling, which provides a central contribution to the unidirectionality. It is interesting to inquire how the matrix elements V_{BH} contribute to the unidirectionality. Second, some mechanistic aspects of superexchange mediated charge separation require information on the individual matrix elements, which appear in eq I.4 and I.5. Information on the ratio $|V_{PB}(L)/V_{BH}(L)|^2$ is necessary to estimate the energetic parameters required to ensure the dominance of the superexchange mediated unistep electron transfer ^{1}P*BH → P$^+$BH$^-$ over the thermally activated ^{1}P*BH → P$^+$B$^-$H process.

(3) (a) Michel, H.; Epp, O.; Deisenhofer, J. *EMBO* **1986**, *5*, 2445. (b) Michel, H.; Deisenhofer, J., private communication.
(4) Martin, J.-L.; Breton, J.; Hoff, A. J.; Migus, A.; Antonetti, A. *Proc. Natl. Acad. Sci. U.S.A.* **1986**, *83*, 957.
(5) Breton, J.; Martin, J.-L.; Migus, A.; Antonetti, A.; Orszag, A. *Proc. Natl. Acad. Sci. U.S.A.* **1986**, *83*, 5121.
(6) (a) Haberkorn, R.; Michel-Beyerle, M. E.; Marcus, R. A. *Proc. Natl. Acad. Sci. U.S.A.* **1979**, *76*, 4185. (b) Marcus, R. A. *Chem. Phys. Lett.* **1987**, *133*, 471. (c) Marcus, R. A., private communication. (d) Marcus, R. A. *Chem. Phys. Lett.* **1988**, *146*, 13.
(7) Fischer, S. F.; Scherer, P. D. J. *Chem. Phys.* **1987**, *115*, 151.
(8) Michel-Beyerle, M. E.; Plato, M.; Deisenhofer, J.; Michel, H.; Bixon, M.; Jortner, J. *Biochem. Biophys. Acta* **1988**, *932*, 52.
(9) (a) Woodbary, N. W.; Becker, M.; Middendorf, D.; Parson, W. W. *Biochemistry* **1985**, *24*, 7516. (b) Fischer, S. F.; Nussbaum, I.; Scherer, P. O. J. In *Antennas and Reaction Centers of Photosynthetic Bacteria*; Michel-Beyerle, M. E., Ed.; Springer: Berlin, 1985; p 256. (c) Jortner, J.; Michel-Beyerle, M. E. In *Antennas and Reaction Centers of Photosynthetic Bacteria*; Michel-Beyerle, M. E., Ed.; Springer: Berlin, 1985; p 345. (d) Jortner, J.; Bixon, M. In *Protein Structure Molecular and Electronic Reactivity*; Austin, R., Buhks, E., Chance, B., De Vault, D., Dutton, P. L., Frauenfelder, H., Gol'danskii, V. I., Eds.; Springer-Verlag: New York, 1987; p 277.
(10) Hoff, A. J. *Photochem. Photobiol.* **1986**, *43*, 727.
(11) (a) Moehl, K. W.; Lous, E. J.; Hoff, A. J. *Chem. Phys. Lett.* **1985**, *121*, 22. (b) Hunter, D. A.; Hoff, A. J.; Hore, P. J. *Chem. Phys. Lett.* **1987**, *134*, 6.
(12) Ogrodnik, A.; Remy-Richter, N.; Michel-Beyerle, M. E.; Feick, R. *Chem. Phys. Lett.* **1987**, *135*, 576.
(13) Peters, K.; Avouris, Ph.; Rentzepis, P. M. *Biophys. J.* **1978**, *23*, 107.
(14) Paschenko, V. Z.; Korvatovskii, B. N.; Kononenko, A. A.; Chamorovsky, S. K.; Rubin, A. B. *FEBS Lett.* **1985**, *191*, 245.
(15) Woodbury, N. W.; Becker, M.; Middendorf, D.; Parson, W. W. *Biochemistry* **1985**, *24*, 7516.
(16) (a) Bixon, M.; Jortner, J.; Michel-Beyerle, M. E.; Ogrodnik, A.; Lersch, W. *Chem. Phys. Lett.* **1987**, *140*, 626. (b) Bixon, M.; Jortner, J.; Michel-Beyerle, M. E. In *Photosynthetic Bacterial Reaction Center: Structure and Dynamics*; Breton, J., Vermiglio, A., Eds.; NATO ASI Plenum Press: New York, 1988, in press. (c) Michel-Beyerle, M. E.; Bixon, M.; Jortner, J., to be published.
(17) Jortner, J. *J. Am. Chem. Soc.* **1980**, *102*, 6676.
(18) Marcus, R. A. *J. Chem. Phys.* **1956**, *24*, 966, 979.
(19) Levich, V. G. *Adv. Electrochem. Eng.* **1965**, *4*, 429.

Table I. Test of the Overlap Approximation Electron Transfer between Aromatic Molecules in Organic Crystals[a]

molecules	config	C_0 Coulomb	K_1 exchange	$C_0 + K_1$	S SCF-AO	S single slater $\zeta = 3.08$ Å^{-1}
naphthalene	(0, b, 0) $R_{cc} = 6.003$ Å	17.6	43.6	61.2	−9.67	−3.44
naphthalene	($a/2$, $b/2$, 0) $R_{cc} = 5.095$ Å	−41.9	−101.7	−143.6	19.26	8.88
anthracene	(0, b, 0) $R_{cc} = 6.036$ Å	57.3	123.5	180.8	−27.23	−10.63
anthracene	($a/2$, $b/2$, 0) $R_{cc} = 5.23$ Å	−100.1	−225.2	−325.3	47.13	17.98

[a] All energies in cm^{-1}, overlap integrals in units of 10^{-4}.

Some semiempirical computational methods were recently advanced for the estimates of intermolecular electron-transfer integrals which induce electron-transfer processes in the RC.[7,20,21] The reliability of such semiempirical methods cannot be readily assessed. In this paper we shall use the intermolecular overlap approximation recently advanced by us[8] to obtain information regarding the relative magnitudes of the electronic transfer integrals. Although this method also falls into the category of semiempirical techniques, its advantages are twofold. First, it rests on a set of systematic, well-defined approximations. Second, previous experience in the area of band structure calculations for excess electron and hole states in organic molecular crystals[22-24] indicates that the overlap approximation provides a reasonable approximation for the relative magnitudes of the intermolecular one-electron-transfer integrals. It does appear that this approximation can be applied to unravel some of the details of the intermolecular electronic interactions responsible for charge separation in the RC.

II. The Intermolecular Overlap Approximation

The calculation of the electron-transfer integrals V_{PB} and V_{BH} rests on the following approximations: (1) The one-electron approximation is used. (2) Many electron intermolecular exchange contributions are apparently neglected. (3) The intermolecular integrals are calculated by using the tight binding approximation with SCF-MO wave functions.

Approximations 1 and 2 together with eq I.3 imply that the intermolecular electronic couplings are reduced to the one-electron integrals

$$V_{PB} = \int d\tau_1\, \psi^P(1) G_{PB} \psi^B(1)$$
$$V_{BH} = \int d\tau_1\, \psi^B(1) G_{BH} \psi^H(1) \qquad \text{(II.1)}$$

where ψ^P is the highest half-filled orbital on $^1P^*$, ψ^B and ψ^H are the LUMOs on B and H, respectively, and G_{PB} and G_{BH} represent the Coulomb interaction between $^1P^*$ and B and between B^- and H, respectively. We would like to note at this point that approximation 2 can be relaxed to incorporate the effects of intermolecular exchange. The intermolecular electronic coupling integrals can be formally expressed in the general form[23,24] $V_{XY} = \int d\tau_1 d\tau_2\, \psi^X(1)\, \hat{G}_{XY}(1,2) \psi^Y(1)$, with X,Y = P,B and H and where $\hat{G}_{XY}(1,2)$ is the sum of the intermolecular Coulomb and exchange operators.[23,24] However, for the sake of the presentation of our approximation, such an elaborate scheme is not necessary, as long as one bears in mind that eq II.1 can be extended to include also the contribution of intermolecular exchange. To proceed, we shall utilize approximation 3, which allows us to set

$$\psi^P = \sum_i C_i^P \phi_i^P \qquad \psi^B = \sum_j C_j^B \phi_j^B \qquad \psi^H = \sum_k C_k^H \phi_k^H \qquad \text{(II.2)}$$

where C_i^P, C_j^B, and C_k^H are the coefficients of the highest half-occupied atomic orbitals i on $^1P^*$, j on B^-, and k on H^-, respectively, while ϕ_i^P, ϕ_j^B, and ϕ_k^H are the atomic orbitals on atom i of $^1P^*$, atom j of B^-, and atom k of H^-, respectively. Equations II.1 and II.2 result in

$$V_{PB} = \sum_i \sum_j C_i^P C_j^B H_{ij}^{PB} \qquad V_{BH} = \sum_j \sum_k C_j^B C_k^H H_{jk}^{BH} \qquad \text{(II.3)}$$

where the interatomic electronic interaction integrals are

$$H_{ij}^{PB} = \int d\tau_1\, \phi_i^P G_{PB} \phi_j^B \qquad H_{jk}^{BH} = \int d\tau_1\, \phi_j^B G_{BH} \phi_k^H \qquad \text{(II.4)}$$

Equation II.3 is now considerably simplified by invoking the intermolecular overlap approximation.

(4) The matrix elements H_{ij}^{PB} and H_{jk}^{BH} were taken to be proportional to the intermolecular overlap integrals S_{ij}^{PB} of the atomic orbitals i and j, and S_{jk}^{PB} of the atomic orbitals j and k, respectively, and is in analogy to the parametrization of nondiagonal matrix elements (resonance integrals) in the conventional INDO procedure.[25]

$$H_{ij}^{PB} = K S_{ij}^{PB} \qquad H_{ij}^{BH} = K S_{jk}^{BH} \qquad \text{(II.5)}$$

where

$$S_{ij}^{PB} = \int d\tau_1\, \phi_i^P \phi_j^B \qquad S_{jk}^{BH} = \int d\tau_1\, \phi_j^B \phi_k^H \qquad \text{(II.6)}$$

and where K is a constant.

The V_{PB} and V_{BH} integrals in eq II.3 are thus approximated by

$$V_{PB} = K S_{PB} \qquad V_{BH} = K S_{BH} \qquad \text{(II.7)}$$

where

$$S_{PB} = \sum_i \sum_j C_i^P C_j^B S_{ij}^{PB} \qquad S_{BH} = \sum_j \sum_k C_j^B C_k^H S_{jk}^{BH} \qquad \text{(II.8)}$$

The intermolecular overlap integrals S_{PB} and S_{BH} can be considered as attributes for probing structural differences, through their dependence on S_{ij}^{BH} and on S_{jk}^{BH}, and for probing differences in the electronic charge distribution, through their dependence on $(C_i^P C_j^B)$ and on $(C_j^B C_k^H)$.

A cursory examination of the intermolecular overlap approximation, eq II.7, may raise some serious questions regarding the validity of such a semiempirical scheme. We shall provide some evidence for the validity of this approximation, which rests on the result of detailed calculation of intermolecular electron-transfer integrals in organic crystals.[22-24] These electron-transfer integrals are given by the sum of intermolecular Coulomb, C_0, and intermolecular exchange, K_1, integrals, i.e.

$$V = C_0 + K_1 \qquad \text{(II.9)}$$

Detailed expressions for these intermolecular integrals between aromatic molecules were derived and calculations of the C_0 and K_1 integrals were performed with many-electron LCAO wave functions.[22-24] The numerical values of these intermolecular integrals depend crucially on the behavior of the electronic molecular wave function at large distances. The calculations of the C_0 and K_1 integrals between pairs of aromatic molecules utilized SCF

(20) Warshal, A.; Parson, W. *J. Am. Chem. Soc.* **1987**, *109*, 6143.
(21) Fischer, S. F.; Scherer, P. O. J. *Chem. Phys. Lett.* **1987**, *141*, 179.
(22) Katz, J. L.; Rice, S. A.; Choi, S. I.; Jortner, J. *J. Chem. Phys.* **1963**, *39*, 1683.
(23) Silbey, R.; Jortner, J.; Rice, S. A.; Vala, M. T. *J. Chem. Phys.* **1965**, *42*, 733.
(24) Silbey, R.; Jortner, J.; Rice, S. A.; Vala, M. T. *J. Chem. Phys.* **1965**, *43*, 2525.
(25) Pople, J. A.; Beveridge, D. L. *Approximate Molecular Orbital Theory*; McGraw-Hill: New York, 1970.

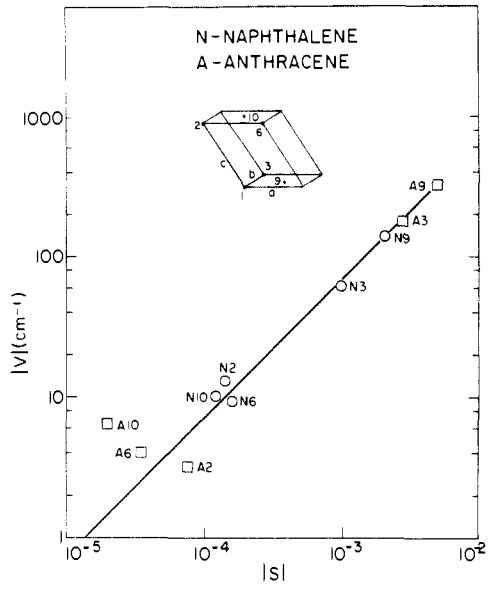

Figure 2. The dependence of the intermolecular electron-transfer integrals V, eq II.9, on the intermolecular overlap S between naphthalene anion radical–naphthalene and anthracene anion radical–anthracene. Both V and S were calculated with LCAO–SCF–AO's (see text). Data from ref 22–24. The intermolecular geometry for pairs of aromatic molecules was taken from the monoclinic crystal structure with two molecules per unit cell (see ref 22). The upper insert in the figure displays the labeling of the molecules J = 2, 3, 6, 9, and 10, which exert the largest V values for the 1 - J interaction. The $|V|$ and $|S|$ data are labeled by NJ for the 1 - J interactions in naphthalene (circles) and by AJ for the 1 - J interaction in anthracene (squares).

atomic orbitals for the construction of the corresponding molecular orbitals (LCAO–SCF–AO) providing an adequate representation of the molecular wave functions at large intermolecular distances.[22-24] These old data[22-24] provide central information regarding the applicability of the intermolecular overlap approximation, which was not explored before. A test of the intermolecular overlap approximation is provided in Table I, which presents numerical results[22-24] for C_0 and K_1 integrals between the pairs of naphthalene anion radical–naphthalene and anthracene anion radical–anthracene molecules at the closest parallel and perpendicular contact in the molecular crystals. The C_0 and K_1 integrals were calculated with LCAO–SCF–AO molecular orbitals. In Table I we also present the intermolecular overlap S calculated using LCAO–SCF–AO, as well as the intermolecular overlap S(sSAO) calculated by representing the molecular orbitals by a linear combination of single Slater atomic orbitals with a single orbital exponent of $\xi = 3.08$ Å^{-1}. From these results the following conclusions are apparent.

(1) Large contributions to V originate from both the intermolecular Coulomb and the intermolecular exchange integrals. Fortunately, in most cases considered by us, the C_0 and K_1 integrals are of the same sign and no cancellation was exhibited.

(2) The larger contribution to V originates from the intermolecular exchange.

(3) The intermolecular overlap calculated with single-Slater AOs is, of course, lower than the S integrals evaluated with the LCAO–SCF–AO.[22-24] Over the relevant distance range the S(sSAO) approximately scales with S, the ratio being S/S(sAO) = 2.5–3.0.

(4) The intermolecular electron-transfer integral, eq II.8, which incorporates both intermolecular Coulomb and exchange, is proportional to the intermolecular overlap integral. In view of conclusion 3 this proportionality can be expressed as $|V| \propto |S|$, or alternatively as $|V| \propto |S(\text{sSAO})|$. In Figure 2 we present the relationship between the values of $|V|$ and the intermolecular overlap integrals S for several pairs of M$^-$–M (M = naphthalene or anthracene) close-lying molecules in the corresponding molecular crystals. We have chosen in each case the closest lying pairs, which are characterized by the largest values of $|V|$ and for

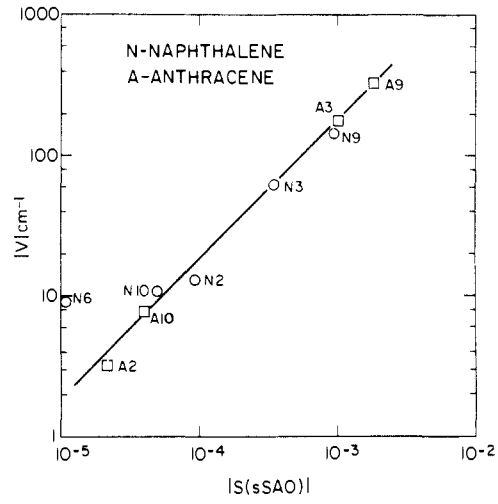

Figure 3. The dependence of the intermolecular electron-transfer integrals V, eq II.9, were calculated with LCAO–SCF–AO's on the intermolecular overlap S(sSAO), which were calculated by representing the π MO's by a linear combination of single Slater orbitals with a single orbital exponent of $\xi = 3.08$ Å^{-1} (see text). Data from ref 22–24. Labels and notation as in Figure 2.

which $|S| = 10^{-4}$ to 5×10^{-3}. These intermolecular electron-transfer integrals, eq II.8, exhibit the empirical relationship

$$|V| = K_0|S| \qquad \text{(II.10)}$$

with

$$K_0 \simeq 8.8 \text{ eV} \qquad \text{(II.10a)}$$

A similar linear relationship is obtained between $|V|$ and the intermolecular overlap S(sSAO) calculated with the single states AOs (Figure 3) for the same pairs of aromatic molecules as in Figure 2. The transfer integrals in Figure 3 exhibit the empirical relation

$$|V| = K|S(\text{sSAO})| \qquad \text{(II.11)}$$

with

$$K \simeq 22 \text{ eV} \qquad \text{(II.11a)}$$

This analysis provides a justification for the intermolecular overlap approximation. It is important to emphasize that on the basis of the data of Figures 2 and 3, the intermolecular overlap approximation, eq II.7 and II.8, although derived for one-electron integrals, incorporates both Coulomb and exchange contributions. Furthermore, one can use the primitive values of S(sSAO) for a characterization of the intermolecular overlap, within the framework of the intermolecular overlap approximation. This procedure will be applied in the next section for the estimate of intermolecular electron-transfer integrals between the prosthetic groups in the RC.

The proportionality constants, eq II.10a or II.11a, derived for pairs of aromatic molecules, may provide the basis for very crude estimates for the numerical values of the intermolecular electron-transfer integrals between prosthetic groups in the RC. However, such absolute values of V derived from eq II.10 or II.11 must be regarded as indicative rather than definite. The rationalization for the application of the intermolecular overlap approximation rests on detailed calculations for simple organic molecular crystals. The semiquantitative information, which emerges for the V vs S relations for pairs of (parallel and nearly perpendicular) aromatic hydrocarbons, cannot be quantitatively applied for intermolecular electronic interactions between prosthetic groups in the RC for two reasons. First, the prosthetic groups also contain heteroatoms in addition to carbon. Second, the interactions between methyl groups are very important. At present, we shall refrain from calculating absolute values of V and utilize the intermolecular overlap approximation for the evaluation of the ratios of the intermolecular electron-transfer integrals between various pigments in the RC.

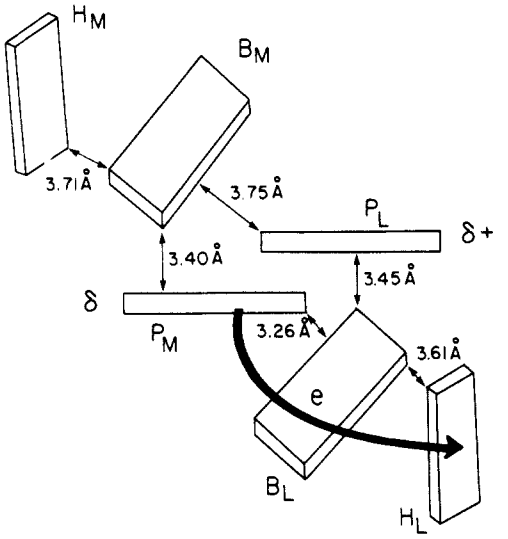

Figure 4. A schematic representation of the intermolecular packing of the pigments in *Rps. viridis*. The shortest heavy-atom–atom distances are marked.

III. Computations

The calculations of the intermolecular overlap integrals, eq II.7, require the LCAO coefficients and the intermolecular atomic overlap integrals. The MO coefficients C_i^P, C_j^B, and C_k^H were taken from the SCF–MO INDO calculations[25,26] by using the X-ray structural data of *Rps. viridis* for the prosthetic groups and for the polar amino acid residues of the protein in their vicinity.[3] As far as intramolecular interactions are concerned, these calculations include the 1s-orbitals of hydrogen atoms, which were attached to the heavy-atom skeleton by standard rules.[25,26] The effect of the polar amino acid residues on the charge distribution of the dimer singlet excitation is substantial. The perturbing electrostatic effect of surrounding polar amino acid residues on the MO's of the dimer has been accounted for by including Coulomb interaction terms of the form $\sum q_j/r_{ij}$ in the Fock matrix, where q_j is the net atomic charge on any amino acid atom j and r_{ij} is the distance from atom i on the dimer and atom j. The values of q_j were taken from the CNDO results of Nemethy, Pottle, and Scheraga on the isolated amino acid residues.[27] Convergence of $S_{PB}(L)$, $S_{PB}(M)$, $S_{BH}(L)$, and $S_{BH}(M)$, within a few percent, was achieved by including all interatomic overlap integrals $|S_{ij}| \geq 1.5 \times 10^{-4}$, while the largest value was $|S_{ij}| \simeq 0.2$. This included some interatomic distances up to 7 Å. The number of terms in eq II.8 amounted to $\sim 10^3$. These MO calculations[26,28] reveal a pronounced charge asymmetry in the highest half-occupied orbital of $^1P^*$, with the orbital charge densities $q_L = 0.30e$, $q_M = 0.70e$ on the "bare" dimer (lacking imposed C_2 symmetry) and $q_L = 0.23e$, $q_M = 0.77e$ on the dimer interacting with the polar protein groups. Individual atomic positions on the dimer show even a larger enhancement in the charge asymmetry by the polar groups. Thus the surplus orbital negative charge density on the M component of the dimer is enhanced by the interaction with the protein polar medium. An orbital charge asymmetry also shows up in the spin density distribution of the radical cation P^+,[26,28] with the reversal of asymmetry in that case.[28]

We have evaluated the intermolecular atomic overlap integrals S_{ij}^{PB} and S_{jk}^{BH} in eq II.7 using INDO Slater orbitals with the single orbital exponents $\xi = 1.2$ au for H, $\xi = 1.625$ au for C(2p) and C(2s), $\xi = 1.95$ au for N(2s) and N(2p), and $\xi = 0.95$ au for the Mg orbitals. It was demonstrated in section II that the utilization of such S(sSAO) intermolecular overlap integrals within the framework of the intermolecular overlap approximation is acceptable. We have used this procedure to evaluate the ratios $V_{PB}(L)/V_{PB}(M)$, $V_{BH}(L)/V_{BH}(M)$, and $V_{BH}(L)/V_{PB}(L)$, where (L) and (M) denote the particular intermolecular interaction between pigments in the L and the M branch, respectively. In what follows we shall denote the two components of the bacteriochlorophyll dimer as P_L and P_M. The accessory chlorophyll B and the bacterioleophytin H along the L and M subunits of the RC are denoted by B_L, H_L and by B_M, H_M, respectively.

The calculation of the intermolecular overlap integrals S_{ij}^{PB} and S_{jk}^{BH} are based on the experimental structural data of *Rps. viridis*,[1-3] with the interatomic coordinates being given at an accuracy of 0.2 Å.[2,3] Inspection of the X-ray data reveals two features of structural asymmetry (Figure 4 and Table II).

(1) The $^1P^*$–B_L and $^1P^*$–B_M Geometry. B_L is closer to the *M*th component of P, which we denote by P_M, than to the *L*th component of P, which is represented by P_L.[1-3] Applying the same notation for the heavy atoms as previously adopted by us[8,26] (Figure 5) we note that the shortest atom–atom distance of 3.26 Å for the pair P_M–B_L involves the methyl carbon atoms C_{2b} and C_{5a}, while the shortest atom–atom distance of 3.45 Å for the pair P_L–B_L involves the O_4–C_{4b} pair with the O_4 dimer atom being 5 bonds away from the π system.[1-3] In addition, the protons on the two methyl groups 2b and 5a on the pair P_M–B_L approach each other as close as 1.9 Å (see Table II). Since these protons form extensions of the π systems by hyperconjugation, they contribute appreciably to the intermolecular overlap integrals. This structural asymmetry of both heavy and light atoms favors the $^1P^*$–B_L interaction over the $^1P^*$–B_M interaction.

Table II. Closest Atom Distances (in Å) between Pigment in the RC of *R. viridis*[a]

pair	heavy atoms	protons[b]
P_L–B_L	3.45 (O_4, C_{4b})	2.08 (H_{1b}, methyl H_{4b})
P_L–B_M	3.75 (O_6, C_{5a})	2.27 (methyl H_2.b, H_{4a})
P_M–B_L	3.26 (C_{2b}, C_{5a})	1.89 (methyl H_{2b}, methyl H_{5a})
P_M–B_M	3.40 (C_9, C_{4b})	2.39 (H_{10}, methyl H_{4b})
B_L–H_L	3.61 (C_{1a}, C_{1a})	1.65 (methyl H_{1a}, methyl H_{1a})
B_M–H_M	3.71 (C_{11}, O_6)	2.29 (methyl H_{1a}, methyl H_{1a})

[a] Phytyl chains truncated as in ref 26. [b] Fixed rotational angle of methyl group (see ref 29).

Table III. Intermolecular Overlap Integrals[a,b] in the RC of *R. viridis*

pair	$10^4\|S\|$	pair	$10^4\|S\|$
P_L–B_L	0.12	P_M–B_M	0.17
P_L–B_M	0.23	B_L–H_L	6.82
P_M–B_L	1.02	B_M–H_M	3.28

[a] Calculated over the highest half-filled MO's of $^1P^*$, B^-, and H^-. [b] Calculated using LCAO of single Slater atomic orbitals.

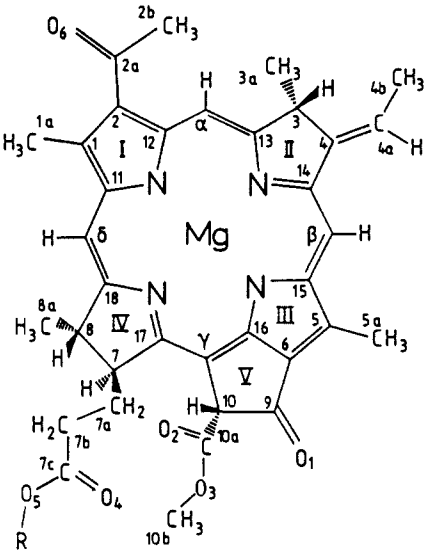

Figure 5. Molecular structure and labeling of atoms of bacteriochlorophyll b.

(26) Plato, M.; Tränkle, E.; Lubitz, W.; Lendzian, F.; Möbius, K. *Chem. Phys.* **1986**, *107*, 185.
(27) Nemethy, G.; Pottle, M. S.; Scheraga, H. A. *J. Phys. Chem.* **1983**, *83*, 1883.
(28) Lubitz, W.; Lendzian, F.; Plato, M.; Tränkle, E.; Möbius, K. *Proc. Colloq. Ampere* **1986**, *23*, 486.

(2) The B_L–H_L and B_M–H_M Geometry. The B_L–H_L shortest heavy-atom separation is smaller than the B_M–H_M nearest heavy-atom distance by 0.1 Å. In both pairs of pigments two methyl groups (1a) are located opposite to each other (Table II). However, the closest approach of protons is 1.65 Å for B_L–H_L and 2.29 Å for B_M–H_M. The structural asymmetry favors the intermolecular interaction V_{BH} between B^- and H across the L branch.

In Table III we summarize the magnitudes of the S_{PB} and S_{BH} intermolecular overlap integrals across the L and M branches,[29] which were used to estimate the relative magnitudes of the intermolecular integrals. These reveal three interesting features.

(1) The electronic coupling between $^1P^*$ and the (mediating) B is enhanced across the L branch by

$$|V_{PB}(L)/V_{PB}(M)|^2 = 7.7 \pm 3.8 \qquad \text{(III.1)}$$

in accord with our previous results.[8] This enhancement of V_{PB} across the L branch originates from the combination of electronic asymmetry, which is due to the surplus negative orbital charge density across the Mth component of $^1P^*$, together with structural asymmetry for the $^1P^*$–B_L and $^1P^*$–B_M geometry. This electronic asymmetry consists of a contribution to eq III.1 of a numerical factor of 2.0 for the bare dimer and of 1.4 for the additional effects of the amino acid residues. The structural contribution to eq III.1 is 3.0.

(2) The coupling between B^- and H is also enhanced across the L branch with

$$|V_{BH}(L)/V_{BH}(M)|^2 = 4.3 \pm 2.0 \qquad \text{(III.2)}$$

This effect originates from the structural asymmetry in the B_L–H_L relative to the B_M–H_M geometries. The large uncertainty in the estimates (III.1) and (III.2) originates from the experimental uncertainites (0.2 Å) in the nuclear coordinates.

(3) The B^-–H coupling is considerably larger than the $^1P^*$–B coupling across both the L and M branches being

$$|V_{BH}(L)/V_{PB}(L)|^2 = 37 \pm 18 \qquad \text{(III.3)}$$

and

$$|V_{BH}(M)/V_{PB}(M)|^2 = 67 \pm 33 \qquad \text{(III.4)}$$

IV. Discussion

The enhancement of the electronic coupling terms V_{PB} and V_{BH} across the L branch of the RC provides an adequate description of the unidirectionality of charge separation across the L branch in bacterial photosynthesis. The asymmetry of the electronic superexchange interaction, eq II.2, across the L and M branches is[8]

$$\psi = |V(L)/V(M)|^2 = |V_{PB}(L)/V_{PB}(M)|^2|V_{BH}(L)/V_{BH}(M)|^2|\delta E(M)/\delta E(L)|^2 \qquad \text{(IV.1)}$$

In the absence of experimental evidence regarding the vertical energy differences across the L and M branches we shall follow our previous analysis[8] and assume that the ratio $\delta E(M)/\delta E(L)$ is close to unity. Equations III.1, III.2, and IV.1 then result in the asymmetry factor of the electronic coupling

$$\psi = 33 \pm 16 \qquad \text{(IV.2)}$$

The total asymmetry in the electron-transfer rates $k(L)$ and $k(M)$ for charge separation across the L and M branches of the RC, respectively, is[8]

$$k(L)/k(M) = \psi r \qquad \text{(IV.3)}$$

where $r = F(L)/F(M)$ is the ratio of the nuclear Franck–Condon factors. In our previous work[8] we have calculated the ratio $F(L)/F(M)$, which originates from electrostatic interactions with the polar glutamate (L104) residue in the vicinity of H_L, together with small differences in Coulomb and polarization energies, to be $r = 1.5$ (+0.8, −0.3). Thus the total asymmetry of the rates, eq IV.3, for the primary charge separation in the RC is

$$k(L)/k(M) = 45\ ^{+55}_{-25} \qquad \text{(IV.4)}$$

This result is in accord with the experimental lower limit $k(L)/k(M) > 10$ for this ratio.[8,30] The dominant contribution to the asymmetry of the rates originates from the electronic coupling. This asymmetry can be traced to four effects: (1) electronic asymmetry of the orbital charge distribution in the highest half-filled MO of the "bare" $^1P^*$, which originates from the dimer structure; (2) enhancement of the electronic asymmetry due to the interaction of $^1P^*$ with the polar protein residues; (3) structural asymmetry originating from small difference in the spatial arrangement of P–H_L relative to P–H_M; and (4) structural asymmetry due to small differences in the B_L–H_L relative to the B_M–H_M spatial arrangement. Effects 1–3 result in the enhancement of $V_{PB}(L)$, eq III.1, while further amplification of the electronic coupling is provided by the enhancement of $V_{BH}(L)$, eq III.2. Effects 3 and 4 are affected by the intermolecular arrangement of both heavy atoms and the hydrogen atoms of the methyl groups. The proximity of methyl groups on neighbor pigments reflects a novel effect of hyperconjugation on intermolecular electron transfer interactions. Thus the unidirectionality of charge separation within the RC essentially originates from "fine tuning" of the "structural engineering" of the prosthetic groups which are arranged in the protein matrix.

To conclude the discussion of the unidirectionality of charge separation in the RC we would like to emphasize that our analysis of this remarkable effect rested on the unistep, superexchange mediated, direct electron transfer. The results of the present calculation of the intermolecular electronic interactions cannot distinguish between the unistep and some of the sequential mechanisms of primary charge separation which were discussed in section I. The two-step sequential electron transfer, which involves the P^+B^-H intermediate, will exhibit asymmetry, favoring the rate of formation of the $P^+B_L^-$ intermediate relative to the $P^+B_M^-$ intermediate by $k_L/k_m = |V_{PB}(L)/V_{PB}(M)|^2 = 7.7 \pm 3.8$, according to relation III.1. This sequential mechanism is rejected on the basis of independent evidence.[16]

The prevalence of the superexchange interaction between $^1P^*$ and P^+H^- does not exclude, in principle, the occurrence of activated electron transfer from $^1P^*$ to P^+B^-, which in the classical limit ($\hbar\omega < k_BT$) proceeds at the crossing of the corresponding potential surfaces (Figure 1). We shall consider the implications of the competition between unistep superexchange and thermally activated electron transfer, which was suggested by Marcus.[16c,d] The ratio of the coupling matrix elements

$$\alpha = |V_{BH}(L)/V_{PB}(L)| \cong 6 \qquad \text{(IV.5)}$$

evaluated in section III is of importance for the estimate of the contribution of the thermally activated channel through a real P^+B^- intermediate. The rate constant of parallel electron transfer to P^+B^- is

$$k_1 = (2\pi V_{PB}^2/\hbar)(4\pi\lambda_1 k_B T)^{-1/2} \exp(-E_a/k_B T) \qquad \text{(IV.6)}$$

The activation energy $E_a = (\Delta G_1 + \lambda_1)^2/4\lambda_1$ can be inferred from the relation $\delta E = \Delta G_1 + \lambda$, where ΔG_1 is the free energy gap between the minima of the $^1P^*$ and P^+B^- potential surfaces, δE is the vertical (free) energy difference between the potential surfaces (Figure 1), and λ_1 is the medium reorganization energy for this process. Accordingly, the activation energy for the parallel process is

$$E_a = \delta E^2/4\lambda_1 \qquad \text{(IV.6a)}$$

The primary electron-transfer process is activationless,[30] with[17]

(29) In these calculations of intermolecular overlap integrals the protons on the methyl groups have been kept in the same fixed position relative to their adjoining π systems for all the pigments. Additional calculations for different rotational angles of the methyl groups were performed. Assuming free rotation of the methyl groups the intermolecular overlap integrals were averaged over the angles to give $\langle(S_{xy})^2\rangle^{1/2}$ ($x \equiv$ P, B and $y \equiv$ B, H). This average value for all pairs PB and BH scales down the former values by factor 2. This constant scaling does not affect our conclusions.

(30) Martin, J. L.; Fleming, G. R.; Breton, J. In *Photosynthetic Bacterial Reaction Centre: Structure and Dynamics*; Breton, J., Vermiglio, A., Eds.; NATO ASI Plenum Press: New York, 1988, in press.

(31) Bixon, M.; Jortner, J. *J. Phys. Chem.* **1986**, *90*, 3795.

$\Delta G \simeq \lambda$. Equations I.1–I.3 result in

$$k \simeq (2\pi V^2/\hbar)(4\pi\lambda k_B T)^{-1/2} \qquad \text{(IV.7)}$$

with the electronic coupling V being given by eq I.4. The ratio k_1/k of the rate constants for the activated channel and the superexchange channel is obtained from eq IV.6 together with eq IV.7 and I.4. Although the medium reorganization energies for the direct superexchange k (λ = 1500–2500 cm^{-1})[16] and for the thermally activated rate k_1 (λ_1) are not necessarily equal, we shall set $(\lambda/\lambda_1)^{1/2} = 1$ in k_1/k as it can be readily shown that this approximation does not grossly modify the estimates of the electronic coupling terms and the vertical energy emerging from our analysis. Accordingly, we obtain

$$\frac{k_1}{k} = \left(\frac{\delta E}{V_{BH}}\right)^2 \exp(-E_a/k_B T) \qquad \text{(IV.8)}$$

The experimental value of the activationless primary electron transfer rate $k = 3.7 \times 10^{11}$ s^{-1},[4,5] which is attributed to superexchange, implies that the electronic matrix element is according to eq IV.7 and I.4

$$V_{PB}V_{BH}/\delta E = (25 \pm 5) \text{ cm}^{-1} \qquad \text{(IV.9)}$$

Equations IV.5–IV.9 result in

$$\frac{k_1}{k} = \left(\frac{\delta E}{25\alpha}\right) \exp[-(\delta E)^2/4\lambda_1 k_B T] \qquad \text{(IV.10)}$$

where $\alpha = V_{BH}/V_{PB}$. This result immediately implies that the enhancement of the B^-H–BH^- coupling relative to the $^1P^*B$–P^+B^- coupling retards the direct activated channel. Equation IV.10 has the form $(k_1/k) \equiv (\delta E) \exp(-\beta(\delta E)^2)$, where β is temperature dependent, indicating that although the increase of δE reduces the superexchange rate k, it also retards the thermally activated channel. Equation IV.10 implies that when the direct process dominates, i.e., $k_1/k \leq 0.2$, the following relation between the parameters does hold

$$\lambda_1 \leq (\delta E)^2/[4k_B T \ln (\delta E/5\alpha)] \qquad \text{(IV.11)}$$

Figure 6 displays the interrelationship between the lower limit for the vertical energy δE and the upper limit for λ_1 according to eq IV.11. It is apparent that the medium reorganization energy cannot be too small. For "reasonable" values of λ_1, i.e., λ_1 = 800 cm^{-1}, this analysis implies that the energetics is not very sensitive to the value of λ_1. It should be borne in mind that these estimates of δE rest on the harmonic approximation. Deviations of the potential surfaces of the protein from harmonicity may result in a considerable decrease of δE. The present analysis, within the framework of its inherent limitations, sets some rough limits on the electronic coupling matrix elements, which ensure the dominance of the temperature-independent superexchange channel (Figure 6). These are given by $V_{PB} = (25\delta E/\alpha)^{1/2}$ and $V_{BH} = (25\alpha\delta E)^{1/2}$. For example, for λ_1 = 800 cm^{-1} and $\delta E \geq$ 1600 cm^{-1} our analysis implies that V_{PB} = 80 cm^{-1} and V_{BH} = 480 cm^{-1}. At present, there is no way to confront these estimates with reliable calculations of absolute values of the intermolecular matrix elements in the RC. Calculations of the band structure of excess

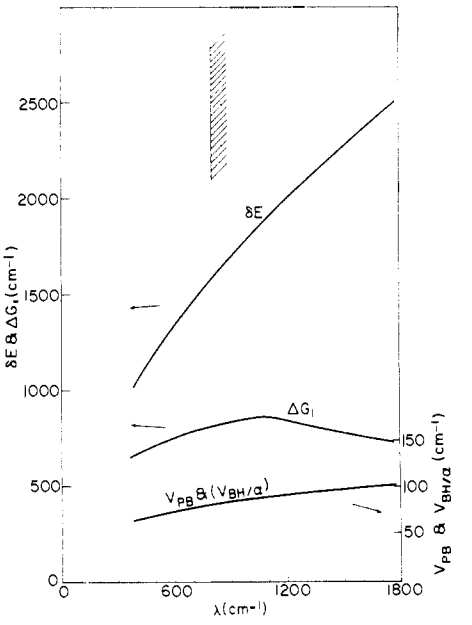

Figure 6. The interrelationship between the energetic parameters δE (and ΔG_1) and the medium reorganization energy, λ, for the activated electron transfer channel, which are required to ensure the dominance of the temperature-independent superexchange channel. The "reasonable" lower limit of λ = 800 cm^{-1} is marked. The rough estimates of the electronic matrix elements V_{PB} and V_{BH} emerging from this analysis are also presented (see text).

electron and hole states in organic crystals of aromatic molecules, which include effects of many-electron exchange,[22-24] indicate that the largest intermolecular transfer integrals are in the range 100–400 cm^{-1}. Thus the estimates of the matrix elements may be reasonable. The next step in the theoretical analysis should address this problem. The energetic parameters originating from our analysis imply that the superexchange mediated direct transfer process from $^1P^*$ to P^+H^- dominates over the thermal process for $^1P^*$ to P^+B^- provided that δE exceeds 1600–2000 cm^{-1} while $\Delta G_1 \gtrsim$ 800 cm^{-1}. Thus the potential surfaces for $^1P^*$ and P^+B^- are reasonably well separated in energy, relative to the characteristic vibrational (mean) protein frequency[31] $\hbar\omega$ = 100 cm^{-1}, with the energy gap corresponding to $\sim 8\hbar\omega$ while the vertical energy is $(16–20)\hbar\omega$. Such relatively large separation proximity effects between $^1P^*$ and P^+B^- potential surfaces will be negligible. Furthermore, small changes between the relative location of these potential surfaces in *Rps. viridis* and *Rb. sphaeroides* are not expected to result in a gross modification of the electron transfer dynamics, providing a rationalization for the similarity of the primary rates in the RCs of these two bacteria.

Acknowledgment. This research was supported by the Deutsche Forschungsgemeinschaft (M.E. MB within Sonderforschungsbereich 143 and M.P. and K.M. within Sonderforschungsbereich 337). J. Jortner would like to express his gratitude for the generous support by the Z. Weinberg Research Fund for Chemical Physics at Tel-Aviv University.